level and its application as an elementary basis for the creaton of various types of automated-design systems.

NOTATION

$\bar{U}_i$, mean velocity in i-th direction; u_i', velocity pulsations in i-th direction; $\bar{C}_k$, mean concentration of k-th component; $\bar{T}$, mean temperature; ρ, density; c_p, specific heat at constant pressure; μ, viscosity of heat carrier; Pr, Prandtl number; Pr_D, diffusional Prandtl number; R_k, heat source (sink) on account of chemical reactions; d_e, equivalent diameter; S_T, mass source (sink) in chemical reaction; $\bar{P}$, mean pressure; n, vector normal; β, volume-expansion coefficient; k, kinetic energy of turbulence; ε, dissipation rate of kinetic energy of turbulence; ∇^2, Laplacian operator; I, pulsations of a scalar quantity; Φ, instantaneous or mean value of a scalar quantity.

LITERATURE CITED

1. N. I. Buleev, Heat Transfer [in Russian], Moscow (1962), pp. 64-98.
2. V. Rodi, Methods of Calculating Turbulent Flow [Russian translation], Moscow (1984), pp. 227-322.
3. B. E. Lounder and D. B. Spolding, Comp. Meth. Appl. Mech. Eng., No. 3, 269-280 (1974).
4. V. I. Nikolaev, V. A. Nemtsev, and L. N. Shegidevich, Vestsi AN BSSR, Ser. Fiz.-Énerg. Navuk, No. 1, 43-47 (1987).
5. O. Zenkevich, Finite-Element Method in Engineering [in Russian], Moscow (1975).
6. A. A. Mikhalevich, V. I. Nikolaev, and V. I. Fedosova, Inzh.-Fiz. Zh., 57, No. 2, 246-253 (1989).

DYNAMICS OF Z-PINCH WITH A LIGHT LINER.

1. DESCRIPTION OF THE MODEL AND CALCULATION OF DOUBLE-SHELL LINERS

G. S. Romanov, A. S. Smetannikov, Yu. A. Stankevich, and V. I. Tolkach

UDC 533.9

The compression of a plasma by a plastic liner has been modeled computationally in the one-dimensional magnetic radiation gasdynamic approximation. The dynamics of the process has been considered with allowance for the deviation from local thermodynamic equilibrium.

Intensive studies have been under way on the compression of a plasma by cylindrical shells (liners), driven toward the symmetry axis by the pressure of the intrinsic magnetic field. These studies have been stimulated by the potential extensive applications in obtaining plasmas with high parameters, producing ultrastrong pulsed magnetic fields, etc. High-power sources of short-wavelength radiation, arising as a result of thermalization of the kinetic energy when the liner "stops" at the axis, have been developed on this basis. Considerable progress in the studies has been made by using high-power nanosecond electrical generators as the power supply [1]. The generated current pulses of several megaamperes with a length of the order of 100 nsec allow the liner to be accelerated to velocities of several hundreds of kilometers per second (light liners with a mass of ~100 μg/cm and an initial radius of ~1 cm). These studies call for a detailed investigation of the physics of the processes, which is very difficult to carry out experimentally. Of particular interest in such problems is the efficiency with which energy from the power supply is converted to the kinetic energy of the linear and then to radiant energy. Moreover, by means of simple analytical solutions it is possible to consider only individual aspects of the compression.

Scientific-Research Institute of Applied Physical Problems, V. I. Lenin Belorussian State University, Minsk.

Translated from Inzhenerno-Fizicheskii Zhurnal, Vol. 59, No. 3, pp. 479-487, September, 1990. Original article submitted April 3, 1990.

0022-0841/90/5903-1178$12.50

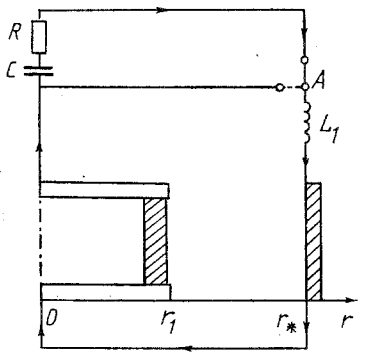

Fig. 1. Electric circuit.

And since many interrelated physical processes must be taken into account for a realistic description of the dynamics of the phenomenon, computational modeling is in fact the only possible way of making a sufficiently complete theoretical study of the picture of the phenomenon.

A system of one-dimensional equations of magnetic radiation gasdynamics (MRGD) in a cylindrical geometry is used to describe the dynamics of plasma compression and heating by a linear [2]:

$$\frac{\partial v}{\partial t} = -r\frac{\partial p}{\partial m} + f; \quad \frac{\partial r}{\partial t} = v; \quad \frac{\partial}{\partial t}\left(\frac{1}{\rho}\right) = \frac{\partial (rv)}{\partial m}; \quad f = -\frac{iH}{\rho};$$
$$\frac{\partial}{\partial t}\left(\frac{H}{\rho r}\right) = \frac{\partial E}{\partial m}; \quad i = \sigma E = \frac{\rho}{4\pi}\frac{\partial (rH)}{\partial m}; \quad \frac{\partial \varepsilon}{\partial t} = -p\frac{\partial (rv)}{\partial m} + \tag{1}$$
$$+ q - \frac{\partial (rS)}{\partial m}; \quad q = \frac{iE}{\rho}; \quad S = \int S_\nu d\nu; \quad S_\nu = \int I_\nu \Omega d\Omega,$$

where $dm = \rho r dr$, $E \equiv E_z$, $H \equiv H_\varphi$, and S is the radiant flux. The electronic thermal conductivity is disregarded since the radiant energy transfer is more significant. The power supply is simulated by ordinary RLC circuit, closed on the liner, with a crowbar breaker A, which is actuated at a time t_*, close to the time of maximum current (Fig. 1). The boundary conditions for Maxwell's equations from system (1) are then determined by the electric circuit equations

$$L_1\frac{dJ}{dt} + RJ - U + lE(r_1, t) = -2l\frac{d}{dt}\left[J\ln\frac{r_*}{r_1(t)}\right];$$
$$\frac{dU}{dt} = -\frac{J}{C}; \quad H(r_1, t) = \frac{2J}{r_1(t)}. \tag{2}$$

Here $r_1(t)$ denotes the boundary of the region in which the current flows, r_* is the radius of the return conductor, and U is the voltage across the capacitor bank. The initial conditions are given in the form $U_{(0)} = U_0$, $I_{(0)} = 0$.

The equations of state of the material, including cold and hot components, are given in the following form to close the gasdynamic equations:

$$p = nkT(1+x) + p_x; \quad n = \sum_z N^z; \quad \varepsilon = \frac{3}{2}\frac{nkT}{\rho}(1+x) + \varepsilon_i + \varepsilon_x;$$
$$x = \left(\sum_z zN^z\right)\Big/ n; \quad \varepsilon_i = \frac{k}{\rho}\sum_z N^z Q_z; \quad Q_z = \sum_{k=1}^{z} I_k; \tag{3}$$
$$p_x = \frac{\rho_0 c_0^2}{m-k}(\delta^m - \delta^k); \quad \varepsilon_x = -\int p_x d\left(\frac{1}{\rho}\right); \quad \delta = \frac{\rho}{\rho_0}.$$

The conductivity necessary for solving Maxwell's equations from system (1) is determined as

$$\sigma^{-1} = \sigma_h^{-1} + \sigma_\ell^{-1}; \quad \sigma_h = \frac{4\sqrt{2}}{\pi^{3/2}} \frac{(kT)^{3/2}\beta}{\sqrt{m}e^2\zeta\Lambda}; \quad \beta = \frac{\zeta + 0.85}{\zeta + 2.18};$$

$$\sigma_\ell = \frac{2}{3}\sqrt{\frac{2}{\pi}} \frac{N_e e^2}{(mkT)^{1/2}\sum_a n_a \sigma_a^t}; \quad \zeta = \frac{\sum_z z^2 N^z}{\sum_z z N^z}; \tag{4}$$

$$\Lambda = \ln\left[1 + \left(\frac{r_D}{b}\right)^2\right]^{1/2}; \quad b = \frac{\zeta e^2}{3kT}; \quad N_e = xn.$$

Here σ_h corresponds to the Spitzer expression for a high-temperature (highly ionized) plasma and σ_ℓ is the Spitzer expression for a low-temperature (weakly ionized) plasma, in which case electron scattering on neutral atoms is the principal process.

Estimates show that parameters such that the conditions of local thermodynamic equilibrium (LTE) are not satisfied are reached in the liner plasma. In view of this, it becomes necessary to determine the charge (ionization) composition of the plasma from the system of kinetic equations

$$\frac{dN^z}{dt} = N_e(N^{z-1}I^{z-1} - N^z I^z + N^{z+1}R^{z+1} - N^z R^z), \tag{5}$$

where $I^z(R^z)$ are the ionization (recombination) rates of a z-tuply charged ion, summed over the levels, and N^z is the concentration of ions of multiplicity z. The rate of electron-collision ionization from a level is found from the Lotz formula (in $cm^3 \cdot sec^{-1}$)

$$I_n^z = 3.14 \cdot 10^{-6} T^{-3/2} q_n^z E_1(x)/x, \quad x = E_n^z/kT,$$

here q_n^z is the number of equivalent electrons in the shell; $E_1(x)$ is an integral exponent; and E_n^z is the energy of ionization from the n-th level. Triple recombination, photorecombination, and dielectronic recombination have been taken into account, i.e.,

$$R^z = R_3^z + R_p^z + R_d^z.$$

The triple recombination rate is determined by the balance with electron-collision ionization:

$$R_3^z = \frac{N_e}{S_1} \frac{g^z}{g^{z+1}} I^z \exp(x), \quad S_1 = 2\left(\frac{mkT}{2\pi\hbar^2}\right)^{3/2},$$

where g^z is the statistical sum of the z-tuply charged ion. The photorecombination rate is calculated using the modified hydrogenlike approximation ($cm^3 \cdot sec^{-1}$):

$$R_p^z = 5.2 \cdot 10^{-14} z x^{3/2} E_1(x) \exp(x), \quad x = E_n^z/kT.$$

The dielectronic recombination rate is found from the approximations suggested in [3]:

$$R_d^z = 10^{-13} Q(a_0, a_1) A\beta^{3/2} \exp(-\beta\chi), \quad \beta = \frac{(z+1)^2 Ry}{kT}.$$

The population of the excited levels was assumed to be related only to the ground state and to adjust to its population instantaneously (quasisteady-state):

$$N_1 C_{12} = N_2(A_{21} + C_{21}),$$

where 1 denotes the ground state and 2 denotes the excited state. The electronic deexcitation rate is determined by the semiempirical Van Rejemorter formula

$$C_{21} = 1.58 \cdot 10^{-5} \frac{g_1}{g_2} \frac{N_e}{\sqrt{T}E_{21}} f_{12} p\left(\frac{E_{21}}{kT}\right),$$

p(x) is given in tables for atoms and ions [3]. The collisional deexcitation rate is related by the condition of detailed balance with the excitation rate

$$C_{21} = \frac{g_1}{g_2} \exp(-E_{21}/kT) C_{12}.$$

The spontaneous transition probability is (sec^{-1}):

$$A_{21} = 4.315 \cdot 10^7 \frac{g_1}{g_2} E_{21}^2 f_{12}.$$

Although this separation of the charge and level kinetics is approximate, it must be introduced. Otherwise the calculation of the charge state and the population of the levels becomes so long that such calculation together with the gasdynamic equations becomes virtually impossible.

The energy transfer by radiation is calculated with allowance for photorecombination and bremsstrahlung processes. The transfer equation then has the form [4]

$$\frac{dI_\nu}{ds} = -\varkappa_\nu I_\nu + j_\nu, \quad j_\nu = \varkappa_\nu^1 I_\nu^p, \quad \varkappa_\nu = \varkappa_\nu^\Phi + \varkappa_\nu^\tau; \quad \varkappa_\nu^1 = \varkappa_\nu^* + \varkappa_\nu^\tau,$$

$$\varkappa_\nu^\Phi = \sum_z \sum_i (N_i^z - N_i^{z*}\Psi)\,\sigma_{\nu,i}^z; \quad \Psi = \exp\left(-\frac{h\nu}{kT}\right), \tag{6}$$

$$\varkappa_\nu^* = \sum_z \sum_i N_i^{z*}\,(1-\Psi)\,\sigma_{\nu,i}^z; \quad \varkappa_\nu^\tau = \frac{AN_e}{(kT)^{7/2}} \sum_z z^2 \frac{N^z}{x^3}(1-\Psi),$$

$$N_i^{z*} = \frac{N_e N_1^{z+1} g_i^z}{S_1 g_1^z} \exp\left[(I^z - E_i^z)/kT\right], \quad x = \frac{h\nu}{kT}, \quad A = \frac{16\sqrt{2}}{3\sqrt{3}} \frac{\pi^{5/2} e^6 \hbar^2}{cm^{3/2}},$$

where photoionization cross section for a z-tuply charged ion in the i-th state $\sigma_{\nu,i}^z$ is taken in the Kramers approximation and allowance is made for the possibility of photoionization from inner shells, for which $\Psi = 0$.

The angular distribution of the intensity I_ν in (6) was taken into account in the forward–reverse approximation for a cylindrical geometry [5]. The resulting equations are averaged with respect to frequency and are solved in the multigroup approximation with the introduction of M photon-energy groups.

The calculations were carried out for plastic liners with the composition $C_9O_{10}N_2$ (ρ_0 = 0.9 g/cm^3, c_0 = 3.65 km/sec, m = 3.5, and k = 2.5); the liner dimensions corresponded roughly to experiments on the Angara-5a device [6-8] and varied within the limits: M = 50-200 μg, ℓ = 1 cm, and r_0 = 0.9-1.5 cm. The power-supply parameters were chosen so that the current reached a maximum of 1-3 MA in a time of 50-100 nsec.

Specifically, we discuss two variants of calculation of a double-shell liner, formed by two coaxial cylinders.

1. Length ℓ = 1 cm, outer cylinder of radius r_1 = 1.25 cm and mass M_1 = 70 μg, and inner cylinder of radius r_2 = 0.95 cm, mass M_2 = 140 μg. The ambient medium is a gas of the same composition as the liner, gas density outside and inside the liner $3.5 \cdot 10^{-6}$ g/cm^3 and between the cylinders, 10^{-6} g/cm^3, C = 0.469 μF, L_1 = 3.2 nH, R = 0.04 Ω, U_0 = 217 kV, r_* = 4 cm, and t_* = 100 nsec. Initial energy margin $E = CU_0^2/2 \approx 11$ kJ.

2. The liner is the same as in variant 1: C = 0.0625 μF, L_1 14 nH, R = 0.01 Ω, U_0 = 1.795 MV, r_* = 4 cm, and t_* = 55 nsec. Initial energy margin E_0 = 100 kJ.

As an example of the calculation, the solid lines in Fig. 2a represent the dependence of the degree of ionization on the density for the range of temperatures obtained from the steady-state kinetics [we set $dN^z/dt \equiv 0$ in Eq. (5)] and those in Fig. 2b represent the temperature dependence of the group absorption coefficients for a set of densities. For comparison, the dashed lines here represent the degree of ionization calculated in the LTE approximation. In the limit of high densities triple recombination predominates and the degree of ionization from the system of Saha equations is reached (LTE). In the region of low densities a coronal equilibrium is attained (photorecombination and dielectronic recombination predominate) and the degree of ionization does not depend on the electron density. The difference from LTE is substantial in this region. In the calculation we used ten spectral groups with the following photon-energy limits: 1–29.6–54.9–77.5–138–552–739–871–4104–8000–40,000 eV.

The absorption coefficients are averaged with respect to frequency in much the same way as Planck averaging, but for the nonequilibrium case

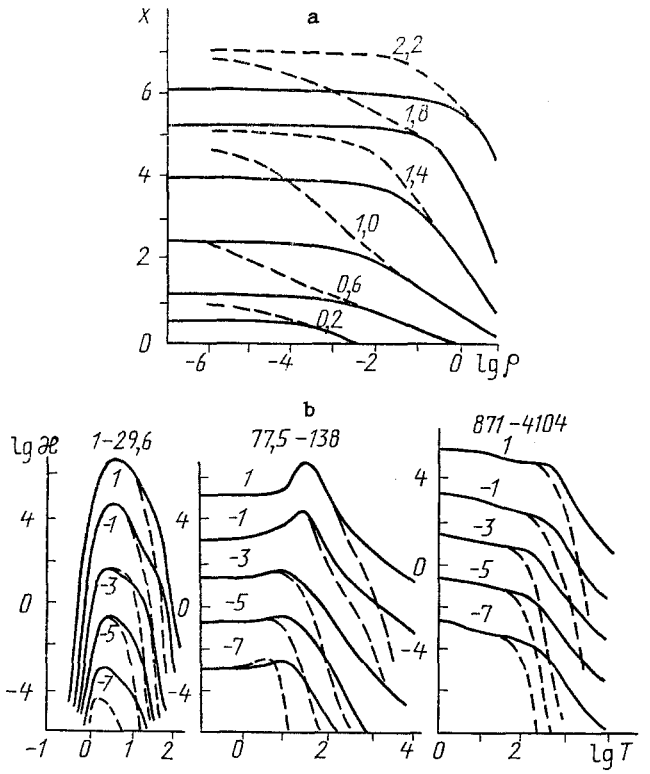

Fig. 2. Dependence of the degree of ionization on the density (a) and of the absorption coefficients on the temperature (b): a) the numbers to the curves are log T. The solid lines represent steady-state kinetics, the dashed curves were obtained from the Saha equations (LTE); b) the numbers to the curves are log ρ. The first (1–29.6 eV), fourth (77.5-138 eV), and eighth (871–4101 eV) spectral groups are given. T, eV; ρ, g/cm^3; ϰ, cm^{-1}.

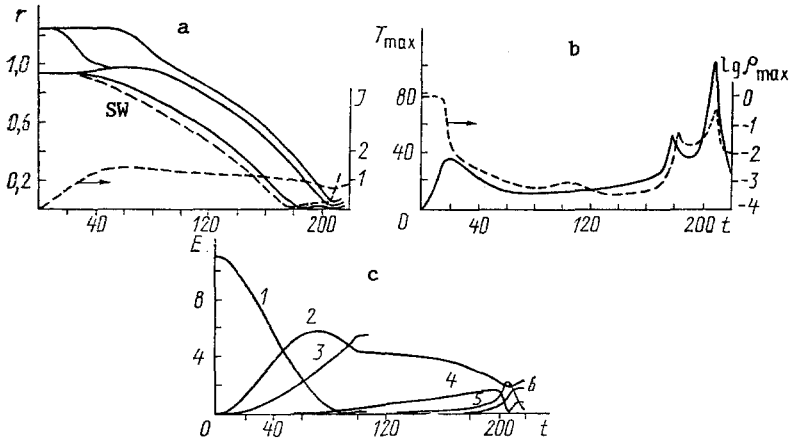

Fig. 3. Time dependence (first variant of calculations) of the current, radii of the contact boundaries of the shells (a), maximum temperature and density (b), energy (c) of capacitance (1), inductance and magnetic field (2), heating of external resistance (3), as well as kinetic (4), internal (5), and radiated (6) energy. r, cm; I, MA, t, nsec; E, kJ.

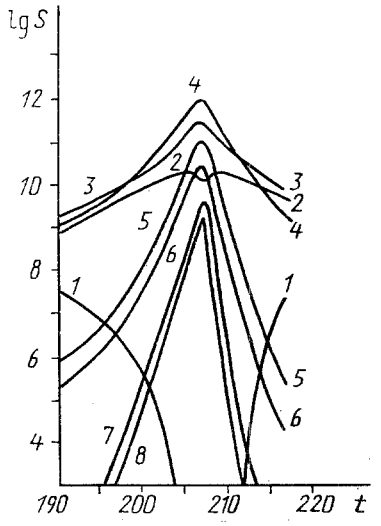

Fig. 4. Time variation of the radiant fluxes in different spectral groups (the numbers are the numbers of the spectral groups). S, W/cm^2; t, nsec.

$$\varkappa_k = \left(\int_{\nu_{k-1}}^{\nu_k} j_\nu d\nu\right) \Big/ \left(\int_{\nu_{k-1}}^{\nu_k} j_\nu/\varkappa_\nu d\nu\right).$$

For a numerical solution the system of MRGD equations (1) and (2) is approximated completely by a conservative difference scheme [2].

Let us consider the results of calculations in the first variant. In an experiment current flow along the liner in the initial interval of time is ensured by an electrical breakdown of the gas. The energy expenditures in the breakdown stage are small, however, and breakdown in fact has little effect on the further development of the phenomenon if azimuthal symmetry is observed (which can be ensured in an experiment). In view of this we do not consider the breakdown kinetics, but we attempt to simulate the breakdown by assigning a value $\sigma_0 \approx 10^{-2}\ \Omega\cdot\text{cm}^{-1}$ to a minimal electrical conductivity σ_0 of the gas. The skin-layer thickness $\delta = c/\sqrt{2\pi\sigma\omega}$ at this value of conductivity is appreciably larger than the initial liner radius. With the onset of discharge of the capacitor bank, therefore, the electric field is uniform inside the liner and the gas heats up almost uniformly. As the current increases (Fig. 3a) the gas in the liner heats up and its electrical conductivity grows. As a result, the skin-layer thickness δ decreases, becomes smaller than the liner radius, and hence the electric field ceases to be uniform — it is maximum in the outer shell of the liner. As a result, the gas on the inside of the outer shell heats up most rapidly, viz., by 15 nsec the temperature here rises to 38 eV. Radiation from this region acts on the shells and evaporates them, i.e., they begin to expand rapidly (Fig. 3a). This produces a shock wave (SW), which travels toward the symmetry axis. The force arising because of the interaction of the current with the magnetic field accelerates the material of the shells toward the symmetry axis and by 40 nsec the inner boundary of the outer shell reaches the inner shell. The outside boundary of each shell does not move for a very long time (up to 50 nsec), since the gas and magnetic pressure gradients here act in opposite directions and almost balance each other. Subsequently, when the current increases (maximum 1.5 MA at 70 nsec), the magnetic-pressure gradient grows and the outside boundaries of the shells also accelerate toward the axis. The gas between the shells is compressed and the inside boundary of the outer shell and the outside boundary of the inside shell move so close to each other that the separation virtually cannot be resolved on the scale of Fig. 3b. This is why, starting from 50 nsec, one line is shown instead of the indicated two contact boundaries of the shells. Radiation in this stage of the discharge plays a major role: the local temperature maximum due to the skin effect is "smeared" by radiation over the material of the shells, heating it almost uniformly to a temperature $T \approx 8$ eV. The maximum temperature in this case decreases from 38 eV at 15 nsec to 10 eV at 70 nsec (Fig. 3b) and the temperature maximum lies on the shock wave. The maximum density in the liner decreases to $\approx 10^{-3}$ g/cm^3 (Fig. 3b). The slight increase in it at 100 nsec is due to the fact that the outside boundary of the outer shell is pressed to the inner boundary and the thickness of the outer shell decreases to 0.05 cm. Next, the liner moves toward the axis as a rather "thick" liner, with a thickness of $\approx$0.4 cm. At 176 nsec the shock wave reaches the symmetry axis and reflects

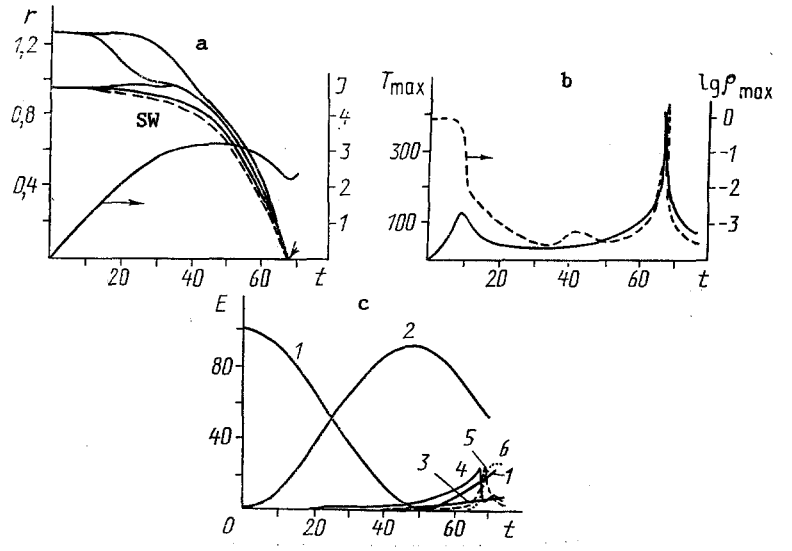

Fig. 5. Time dependence of the positions of the contact boundaries and the current (a), maximum densities and temperatures (b), and the various energy components (c) for the second variant. The notation is the same as in Fig. 3.

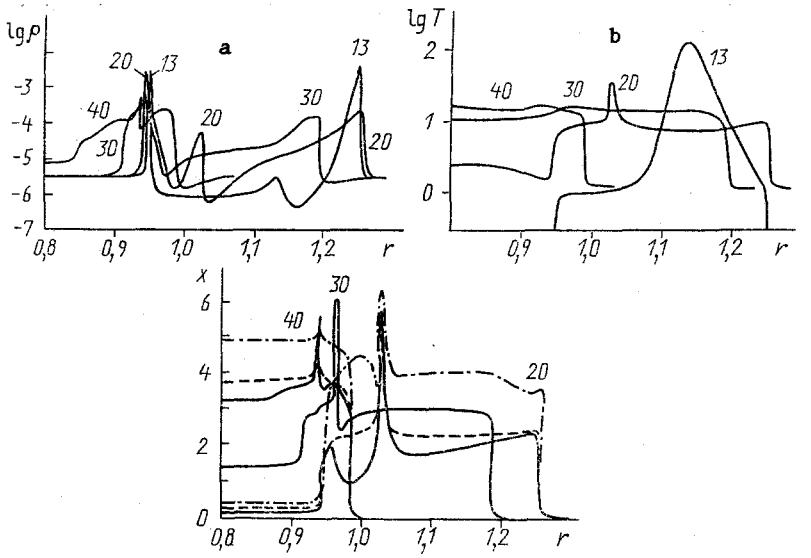

Fig. 6. Radial distributions of the density, temperature, and degree of ionization for several times (the numbers are the time in nsec) for the second variant. The solid, dashed, and dash-dot lines correspond to unsteady and steady-state kinetics and to LTE (Saha).

from it. At that time the maximum temperature on the radius rises to 51 eV and the density to $5\cdot10^{-2}$ g/cm^3. In the stage of convergence the plasma temperature was almost uniform at 10-15 eV with a slight rise at the leading edge of the shock wave. We note that while the outer shell gradually becomes thinner, the inner shell retains a virtually constant thickness until it reaches the symmetry axis. The reflected shock wave travels in the material of the liner and at 206 nsec emerges outside. The liner is compressed most intensively at 208 nsec, with the temperature rising to 104 eV and the density to 0.3 g/cm^3. The material of the liner, reflected from the axis, then begins to expand while the temperature and density decrease. Let us consider the energy characteristics of the discharge as a function of time (Fig. 3c). In the period up to 100 nsec the energy $CU^2/2$ from the capacitance is pumped mainly into the energy $-LJ^2/2 + \int H^2/8\pi dV$ of the inductance (magnetic field) and part of it $\int RJ^2dt$ is lost in the external resistance. The kinetic and internal energies are small and increase slowly with time. The crowbar-breaker is tripped at 100 nsec and as a result the energy stored in the inductance will then be transferred only to the liner. The energy ac-

cumulated in the inductance and transferred to the plasma by the time 100 nsec amounts to 5 kJ, which is about 45% of the initial energy stored E_0. From 100 to 180 nsec the liner gradually accelerates, the kinetic energy increases to 1.5 kJ because of a decrease in the inductance energy, and the internal energy grows much more slowly. Starting from 180 nsec, the internal layers of the liner are slowed down in their motion toward the axis, the growth rate of the internal energy increases, while that of the kinetic energy decreases, although the kinetic energy still grows since the outer layers of the liner have not yet begun to slow down. Subsequently, because the liner has "stopped," the kinetic energy is converted to internal energy, the temperature of the plasma rises, and the plasma begins to radiate intensively. At 208 nsec the internal energy reaches a maximum at 2.2 kJ and then decreases after the liner is reflected from the axis, while the kinetic energy increases. In this interval of time the energy radiated from the liner plasma increases to 1.6 kJ. Thus, roughly 15% of the initial stored energy can be converted to radiation and upon cumulation maximum radiant fluxes are reached in 3-5 spectral groups (Fig. 4).

Let us consider the second variant which qualitatively proceeds in much the same way as the first. Because of the skin effect the gas in the intershell space near the outer shell heats up most. By 10 nsec, the temperature in this region affects the shells and evaporates them; the shells begin to expand rapidly, their density decreases (Fig. 5b), and a shock wave is formed and moves toward the axis (Fig. 5a). The current gradually increases (Fig. 5a) and by 50 nsec reaches a maximum at 3.25 MA. Since the current density is high in the hot region, the magnetic force acting on the plasma in this region is also considerable and as a result the plasma is accelerated toward the axis with a velocity of ≈200 km/sec. Behind it the inside boundary of the outer shell moves with virtually the same velocity and catches up to the inner shell by 25 nsec. The energy transfer by radiation gradually "resorbs" the temperature peak and makes it almost uniform by 30 nsec with a value of ≈15 eV. Starting from 25 nsec, the outside boundary of the liner gradually accelerates and begins to gain on the inner shell. Roughly by 45 nsec the liner becomes rather thick (thickness ≈0.1 cm) and then moves toward the axis, slowly becoming thinner. The time variation of the energy in the various components of the electric circuit is shown in Fig. 5c. An idea of the dynamics of the variation of the plasma parameters is given by Fig. 6, which shows the radial profiles of the density, temperature, and degree of ionization for several times. The degree of ionization, calculated in the LTE approximation (from the Saha equations), is noticeably above the nonequilibrium level while the calculation with steady-state kinetics [$dN^z/dt = 0$ in Eq. (5)] differs little from that with unsteady kinetics. Accelerating gradually, the liner approaches the axis and reaches it at 76.6 nsec. Before that time the velocity is ≈500 km/sec and the temperature (practically uniform from the axis to the outside boundary) is 37 eV. Upon cumulation at the axis the oncoming plasma is retarded, its kinetic energy (≈23 kJ) is converted to internal energy and the gas heats up to a temperature of several hundred electron-volts. In the processes the radiant losses increase and by 68 nsec roughly 22% of the initial stored energy $E_0 = CU_0^2/2$ is emitted by luminescence. The maximum temperature and density at the time of cumulation are 410 eV and 5.25 g/cm^3, respectively. Of course, radiation transfer also plays a certain role in the line spectrum. In this case, the self-consistent problem must be solved with allowance for the interplay of the radiation and the population of the upper levels, and this poses major problems. Moreover, as follows from the results obtained, even when the continuous spectrum (of retardation and photorecombination processes) is taken into account practically all of the kinetic energy is "converted" to radiation.

The results of calculations in the different variants permits the following conclusions. Computational modeling of the liner motion makes it possible to obtain detailed information about its electrical, gasdynamic, optical, and energy characteristics. In the stage when the liner converges toward the axis, the internal energy of the liner is substantially lower than the energy of the inductance (magnetic field) and the kinetic energy. The energy transfer from the power supply to the inductance–liner circuit is fairly efficient and amounts to ≈50% of the initial stored energy. The deviation from local thermodynamic equilibrium during compression of the liner may be substantial and must be taken into account because otherwise incorrect results may be obtained. Virtually all of the kinetic energy acquired by the liner before reflection from the axis (roughly 15-25% of the initial stored energy) is converted to radiation in the vacuum ultraviolet and the shorter-wavelength region. The deviations from LTE have an influence primarily on the optical characteristics and appreciably affect the radiant losses.

NOTATION

r, radius; t, time; m, Lagrangian coordinate; v, velocity; p, pressure; ρ, density; T, temperature; ε, energy of a unit mass; i, current density; E, H, electric and magnetic field strengths; σ, electrical conductivity; I_ν, spectral intensity of the radiation; I, current; R, resistance; L, inductance; U, voltage; C, capacitance; N^z, density of ions with charge z; N_e, electron density; κ_k, group absorption coefficient; q, Joule heating power; f, ponderomotive force; ν, frequency; r_D, Debye radius.

LITERATURE CITED

1. S. G. Alikhanov, L. I. Rudakov, V. P. Smirnov, et al., Pis'ma Zh. Tekh. Fiz., 56, No. 22, 1395 (1979).
2. A. A. Samarskii and Yu. P. Popov, Computational Methods of Solving Gasdynamic Problems [in Russian], Moscow (1980).
3. L. A. Vainshtein, I. I. Sobel'man, and E. L. Yukov, Excitation of Atoms and Spectral Line Broadening [in Russian], Moscow (1979).
4. D. Mihalas, Stellar Atmospheres, 2nd edn., Freeman, San Francisco (1978).
5. G. S. Romanov and A. S. Smetannikov, Zh. Tekh. Fiz., 52, No. 9, 1756 (1982).
6. E. P. Velikhov, K. B. Kartashev, V. D. Ryutov, et al., Vopr. At. Nauki Tekh. Ser. Termoyad. Sintez, No. 1, 3 (1987).
7. S. L. Bogolyubskii, E. M. Gordeev, S. A. Dan'ko, et al., Pis'ma Zh. Tekh. Fiz., 11, No. 20, 1271 (1985).
8. S. L. Bogolyubskii, E. M. Gordeev, Yu. G. Kalinin, et al., BEAMS'88. Proceedings of 7th International Conference on High-Power Particle Beams, Karlsruhe (1988), pp. 1255-1260.

GEOTHERMAL ENERGY UTILIZATION WITH HEAT PIPES

L. L. Vasil'ev

UDC 536.248:536.421.4

Several variants of heat pipes for utilization of geothermal energy and underground rock heat are studied. An original configuration is proposed for a long length vapor-dynamic thermosyphon for such purposes, and experiments performed to test the hypothesis.

Introduction

The planet earth has large energy reserves; however, the thermal flux density per unit surface area is low (0.1-1 kW/m^2). Nevertheless, the earth's surface radiates an energy of $8 \cdot 10^{20}$ J/yr into the surrounding space, which is equivalent to the heat of combustion of $1.9 \cdot 10^{10}$ ton of petroleum.

It is well known that at a depth of 10-20 m the ground temperature is relatively high (10-15°C), independent of seasonal air temperature variations, and increases slowly with depth, reaching 250-300°C at a depth of 4-5 km. The energy stored in the rock strata at such a depth is many times the total heating capability of world reserves of organic fuel. The energy of geothermally heated water within the USSR at temperatures of 30-100°C is about $8.4 \cdot 10^{17}$ J/yr.

Viewed as a heat source, we may arbitrarily divide the earth into three zones having different temperatures: a) surface layers (to 10 m), the temperature of which varies periodically under the action of solar radiation; b) soil and rock of approximately constant temperature, saturated with thermal or ground water; c) deep rock strata.

A. V. Lykov Institute of Heat and Mass Transport, Academy of Sciences of the Belorussian SSR.

Translated from Inzhenerno-Fizicheskii Zhurnal, Vol. 59, No. 3, pp. 488-492, September, 1990. Original article submitted March 19, 1990.

0022-0841/90/5903-1186$12.50